Sub-Leading Effects in Atmospheric Neutrino Oscillations

M. C. Gonzalez-Garcia
C.N. Yang Institute for Theoretical Physics, SUNY at Stony Brook, Stony Brook, NY 11794-3840, USA
IFIC, Universitat de València – C.S.I.C., Apt. 22085, E-46071 València, Spain

Abstract

Atmospheric neutrino oscillations are dominantly due to $\nu_\mu \to \nu_\tau$ flavour mixing. In this workshop we are going to discuss the possibility of observing sub-leading effects on top of the dominant one at present and future atmospheric neutrino experiments. In the framework of three-neutrino mixing, such effects are due to atmospheric ν_e flavour oscillations arising from the θ_{13} mixing and/or from the Δm^2_{21}-induced oscillation wavelength. Other forms of physics beyond the Standard Model, such as, for example, the violation of the equivalence principle, or the violation of Lorentz invariance, can also be a source of sub-dominant atmospheric oscillations. In this talk I will review the basic characteristic features of these different effects as well as their expected size. Observability of these effects depends strongly on the assumed experimental and theoretical systematic uncertainties. Thus, this talk is aimed at setting the ground for most of the following talks and discussions in this workshop.

1. Introduction: Leading $\nu_\mu \to \nu_\tau$ oscillations

As illustration of our present understanding of the dominant source of atmospheric (ATM) neutrino oscillations, I start by presenting in Fig. 1 the result of our 2ν analysis of the ATM neutrino data [1] in terms of $\nu_\mu \leftrightarrow \nu_\tau$ oscillations. The region is perfectly symmetric around $\theta = \pi/4$ since for 2-ν $\nu_\mu \to \nu_\tau$ oscillations, there are no matter effects and the oscillation probability depends on $\sin^2 2\theta$. The best fit point occurs at maximal mixing $\theta = \pi/4$.

This analysis includes the complete 1489-day charged-current data set for Super-Kamiokande (SK)-I, which comprises the sub-GeV and multi-GeV e-like and μ-like contained event samples (each grouped into 10 bins in zenith angle), as well as the stopping (5 angular bins) and through-going (10 angular bins) up-going muon data events. The calculation of the event rates uses the three-dimensional ATM neutrino fluxes given in Ref. [2].

pp. 1–18

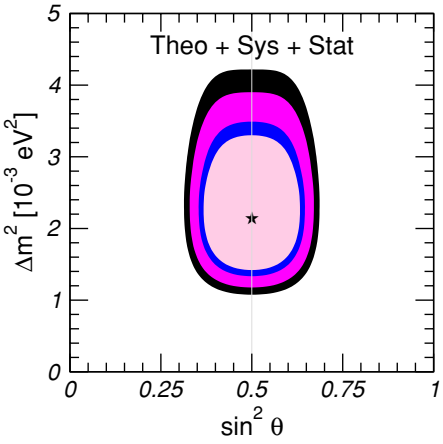

Fig 1. Allowed region for ATM $\nu_\mu \to \nu_\tau$ oscillations.

The statistical analysis applied to the data in order to extract the results in Fig. 1 is based on the *pull* method [3] which has become customary to account for theoretical and experimental systematic uncertainties. In brief the basic idea of the pull method consists in parametrizing the systematic errors and the theoretical uncertainties in terms of a set of variables $\{\xi_i\}$, called pulls, which are then treated on the same footing as the other parameters of the model. The χ^2 function takes the form

$$\chi^2 = \min_{\xi_i}\Big[\sum_{n=1}^{55}\left(\frac{R_n^{\rm theo} - \sum\limits_i \xi_i \sigma_n^i - R_n^{\rm exp}}{\sigma_n^{\rm stat}}\right)^2 + \sum_{i,theory}\xi_i^2 + \sum_{i,syst}\xi_i^2\Big] \qquad (1)$$

where σ_j^i is the error in the observable j due to the uncertainty source i. As illustration, I list here the 18 independent sources of of theoretical and systematic uncertainties included in this analysis [1].

The theoretical uncertainties include uncertainties in the original ATM neutrino fluxes and in the cross-sections. In this analysis the uncertainties of the ATM neutrino fluxes have been parametrized in terms of four pulls: (i) a total normalization error, which we set to 20%; (ii) a "tilt" factor which parametrizes possible deviations of the energy dependence of the ATM fluxes from the simple power law defined as

$$\Phi_\delta(E) = \Phi_0(E)\left(\frac{E}{E_0}\right)^\delta \approx \Phi_0(E)\left[1 + \delta \ln\frac{E}{E_0}\right] \qquad (2)$$

with an uncertainty on the factor δ, $\sigma_\delta = 5\%$ and $E_0 = 2$ GeV; (iii) the uncertainty on the ν_μ/ν_e ratio, which is assumed to be $\sigma_{\mu/e} = 5\%$; and (iv) the uncertainty on

the zenith angle dependence which induces an error in the up/down asymmetry of events which we conservatively take to be 5%.

Cross section uncertainties have been included in the form of (a) three independent normalization errors for the different contributions to the interaction cross section: quasi-elastic scattering (QE), $\sigma^{\sigma_{\rm QE}}_{\rm norm} = 15\%$, single pion production(1π), $\sigma^{\sigma_{1\pi}}_{\rm norm} = 15\%$, and deep inelastic (DIS) scattering (also refer to as multi-pion) $\sigma^{\sigma_{\rm DIS}}_{\rm norm} = 15\%$ for contained events and $\sigma^{\sigma_{\rm DIS}}_{\rm norm} = 10\%$ for upward-going muons; (b) three errors on the flavour ratios $\sigma_{i,\nu_\mu}/\sigma_{i,\nu_e} \sim 0.1$–$1\%$ which are relevant only for contained events, and which are much smaller than the total normalization uncertainties.

Eight sources of experimental systematic uncertainties are included due to: (i) the simulation of the hadronic interactions $\sigma^{\rm sys}_{\rm hadron} = -0.25$–$1.1$ %; (ii) the particle identification procedure, $\sigma^{\rm sys}_{\mu/e} = -1.1$–$1.6\%$; (iii) the ring-counting procedure, $\sigma^{\rm sys}_{\rm ring} = -0.75$–$5.5\%$; (iv) the fiducial volume determination, $\sigma^{\rm sys}_{\rm f-vol} = -0.3$–$1.4\%$; (v) the energy calibration,$\sigma^{\rm sys}_{\rm E-cal} = -0.4$–$2\%$; (vi) the relative normalization between partially-contained and fully-contained events, $\sigma^{\rm sys}_{\rm PC-nrm} = 2.85\%$; (vii) the track reconstruction of upgoing muons, $\sigma^{\rm sys}_{\rm track} = 1.4$–$6.4\%$; and (viii) the detection efficiency of upgoing muons, and the stopping-thrugoing separation, $\sigma^{\rm sys}_{\rm up-eff} = 1$–$1.4\%$.

Other analysis in the literature, including the one from the SK collaboration, include these uncertainties in similar manner, although they differ in the exact size and form of the assumed uncertainties. As we will see in the next talks, this can lead to differences on the possible observability of the sub-leading effects.

2. Three-Neutrino Oscillations

The minimum joint description of ATM, K2K, solar and reactor data requires that all the three known neutrinos take part in the oscillations. The mixing parameters are encoded in the 3×3 lepton mixing matrix which can be conveniently parametrized in the standard form:

$$\begin{pmatrix} 1 & 0 & 0 \\ 0 & c_{23} & s_{23} \\ 0 & -s_{23} & c_{23} \end{pmatrix} \begin{pmatrix} c_{13} & 0 & s_{13}e^{i\delta} \\ 0 & 1 & 0 \\ -s_{13}e^{-i\delta} & 0 & c_{13} \end{pmatrix} \begin{pmatrix} c_{21} & s_{12} & 0 \\ -s_{12} & c_{12} & 0 \\ 0 & 0 & 1 \end{pmatrix}$$

where $c_{ij} \equiv \cos\theta_{ij}$ and $s_{ij} \equiv \sin\theta_{ij}$. There are two possible mass orderings, which we denote as *Normal* and *Inverted*. In the normal scheme $m_1 < m_2 < m_3$ while in the inverted one $m_3 < m_1 < m_2$.

From the analysis of solar and ATM oscillations we know that

$$\Delta m^2_\odot = \Delta m^2_{21} \ll |\Delta m^2_{31}| \simeq |\Delta m^2_{32}| = \Delta m^2_{\rm atm} \, . \tag{3}$$

Generic 3-ν oscillation effects which could be observable in ATM neutrino data include:

- effects due to the mixing angle θ_{13};
- difference between Normal and Inverted schemes;
- coupled oscillations with two different wavelengths;
- CP violation

The strength of these effects is controlled by the values of the ratio of mass differences $\Delta m^2_{21}/|\Delta m^2_{31}|$, by the mixing angle θ_{13}, and by the CP phase δ.

In order to quantify these effects one needs to obtain the oscillation probabilities for ATM neutrinos by solving the evolution equation of the neutrino system in the matter background of the Earth:

$$i\frac{d\vec{\nu}}{dt} = H\,\vec{\nu}, \qquad H = U\cdot H_0^d\cdot U^\dagger + V\ , \tag{4}$$

where $\vec{\nu}\equiv(\nu_e,\nu_\mu,\nu_\tau)^T$, H_0^d is the vacuum hamiltonian,

$$H_0^d = \frac{1}{2E_\nu}\mathrm{diag}\left(-\Delta m^2_{21},0,\Delta m^2_{32}\right), \tag{5}$$

and V is the effective potential that describes charged-current forward interactions in matter:

$$V = \mathrm{diag}\left(\pm\sqrt{2}G_F N_e,0,0\right)\equiv \mathrm{diag}\left(V_e,0,0\right). \tag{6}$$

In Eq. (6), the sign + (−) refers to neutrinos (antineutrinos), and N_e is electron number density in the Earth.

2.1. Effects due to θ_{13}

I will discuss first the sub-leading effect due to the mixing angle θ_{13}. For ATM neutrinos, they are particularly easy to treat in the *hierarchical approximation* in which Δm^2_{21}-induced oscillations are neglected in the ATM neutrino analysis. In this approximation one can rotate away the angle θ_{12} and the resulting survival probabilities do not depend on Δm^2_{21} and θ_{12}. For instance for constant Earth matter density they can be written as follows [4]:

$$\begin{aligned} &P_{ee} = 1-4s^2_{13,m}c^2_{13,m}\,S_{31}, \qquad P_{e\mu} = 4s^2_{13,m}c^2_{13,m}s^2_{23}\,S_{31}, \\ &P_{\mu\mu} = 1-4s^2_{13,m}c^2_{13,m}s^4_{23}\,S_{31} - 4s^2_{13,m}s^2_{23}c^2_{23}\,S_{21} - 4c^2_{13,m}s^2_{23}c^2_{23}\,S_{32}. \end{aligned} \tag{7}$$

Here $\theta_{13,m}$ is the effective mixing angle in matter:

$$\sin 2\theta_{13,m} = \frac{\sin 2\theta_{13}}{\sqrt{(\cos 2\theta_{13} - 2E_\nu V_e/\Delta m^2_{32})^2 + (\sin 2\theta_{13})^2}}\,, \tag{8}$$

$S_{ij} = \sin^2\left(\frac{\Delta\mu^2_{ij}}{4E_\nu}L\right)$ are the oscillating factors in matter, and $\Delta\mu^2_{ij}$ are the effective mass-squared differences in matter:

$$\begin{aligned}
\Delta\mu^2_{31} &= \frac{\Delta m^2_{32}}{2}\left(\frac{\sin 2\theta_{13}}{\sin 2\theta_{13,m}} - 1\right) - E_\nu V_e \ , \\
\Delta\mu^2_{32} &= \frac{\Delta m^2_{32}}{2}\left(\frac{\sin 2\theta_{13}}{\sin 2\theta_{13,m}} + 1\right) + E_\nu V_e, \\
\Delta\mu^2_{31} &= \Delta m^2_{32}\frac{\sin 2\theta_{13}}{\sin 2\theta_{13,m}} \ . \qquad (9)
\end{aligned}$$

The main effect of θ_{13} is that now ATM neutrinos can oscillate simultaneously in both the $\nu_\mu \to \nu_\tau$ and $\nu_\mu \to \nu_e$ (and, similarly, $\nu_e \to \nu_\tau$ and $\nu_e \to \nu_\mu$) channels. The oscillation amplitudes for channels involving ν_e are controlled by the size of $\sin^2\theta_{13} = |U_{e3}|^2$. Furthermore, because of matter effects the size of the effect is different for normal and inverted hierarchies.

In Fig. 2 we show the expected zenith angular distribution of contained e-like events (normalized to the no-oscillation expectation) for $\sin^2\theta_{13} = 0.04$. The results in the figure can be understood as follows. From Eq.(7) we find that for the case of constant matter density the expected flux of ν_e events in the hierarchical approximation is [5, 6, 7]

$$\frac{N_e}{N_{e0}} - 1 = \overline{P}_{e\mu}\bar{r}(s^2_{23} - \frac{1}{\bar{r}}) \, . \qquad (10)$$

$\overline{P}_{e\mu}$ is the corresponding probability, averaged over energy and zenith angle, and $\bar{r} = N_{\mu 0}/N_{e0}$ where N_{e0} and $N_{\mu 0}$ are the expected number of electron and muon-like events in the absence of oscillations in the relevant energy and angular bin. For example, for sub-GeV events, $\bar{r} \sim 2$. Eq. (10) illustrates how these effects break the symmetry around maximal θ_{23} mixing and have, in principle, the potentiality to discriminate the octant of θ_{23}.

As seen in the figure, the effect is mostly relevant for multi-GeV events, for which matter effects lead to an enhancement [5, 6, 7, 8] which is slightly larger for the normal ordering where the matter enhancement is in the neutrino channel. For sub-GeV events, the matter term can be neglected and the effect of a non-vanishing θ_{13} is smaller and it is the same for normal and inverted ordering. Furthermore, due to the $(s^2_{23} - \frac{1}{\bar{r}})$ factor, for θ_{23} in the first (second) octant there is a decrease (increase) in the number of electron events as compared to the $\theta_{13} = 0$, and the effect is suppressed for maximal θ_{23} mixing.

From the previous discussion we conclude that the slight excess of sub-GeV over multi-GeV e-like events, which seems to be observed in the data, cannot be explained by a non-vanishing θ_{13}. Indeed the best fit occurs for very small θ_{13} ($\sin^2\theta_{13} < 0.005$) and maximal θ_{23}.

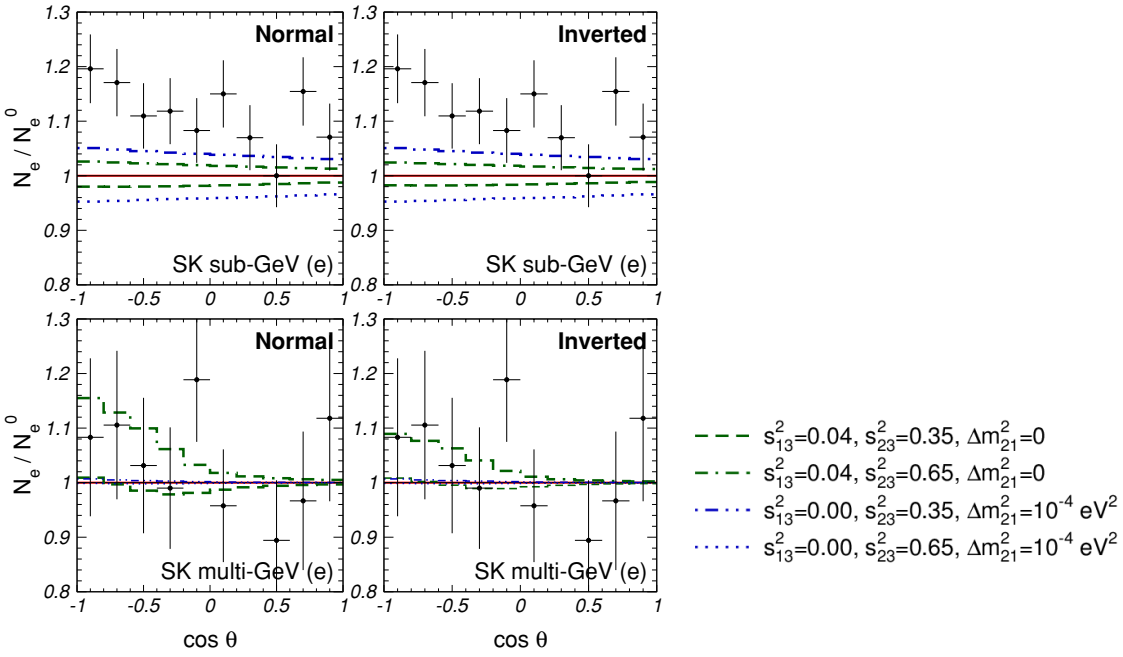

Fig 2. Comparison of the sub-leading effects due to Δm^2_{21}- and θ_{13}-induced ν_e oscillations in the expected zenith angular distribution of e-like events. In all curves $\tan^2\theta_{12} = 0.42$, and $\Delta m^2_{32} = 2.2 \times 10^{-3}$ eV^2.

2.2. Effects due to Δm^2_{21}

I next discuss the sub-leading effects due to Δm^2_{21} oscillations for vanishing small value of θ_{13}. In this approximation and for constant Earth matter density the relevant oscillation probabilities can be written as:

$$\begin{aligned} P_{ee} &= 1 - P_{e2}\,, \qquad P_{e\mu} = c^2_{23} P_{e2}\,, \\ P_{\mu\mu} &= 1 - c^4_{23} P_{e2} - 2 s^2_{23} c^2_{23} \left[1 - \sqrt{1 - P_{e2}\cos\phi}\right]\,, \end{aligned} \tag{11}$$

where

$$P_{e2} = \sin^2 2\theta_{12,m} \sin^2\left(\frac{\Delta m^2_{21}\, L}{4E_\nu} \frac{\sin 2\theta_{12}}{\sin 2\theta_{12,m}}\right)\,, \tag{12}$$

with

$$\sin 2\theta_{12,m} = \frac{\sin 2\theta_{12}}{\sqrt{(\cos 2\theta_{12} \mp \frac{2E_\nu V_e}{\Delta m^2_{21}})^2 + \sin^2 2\theta_{12}}} \tag{13}$$

$$\phi \approx (\Delta m^2_{31} + s^2_{12}\,\Delta m^2_{21}) \frac{L}{2E_\nu}\,. \tag{14}$$

In Fig. 2 I show the angular distribution of ATM ν_e for non-vanishing values of Δm^2_{21}. As seen in the figure, unlike for $\theta_{13} \neq 0$, the main effect of a small but

non-vanishing Δm^2_{21} is mostly observable for sub-GeV electrons. The effect can be understood in terms of the approximate analytical expressions [7, 9, 10]:

$$\frac{N_e}{N_{e0}} - 1 = \overline{P}_{e2}\bar{r}(c^2_{23} - \frac{1}{\bar{r}}), \quad (15)$$

$$\frac{N_\mu - N_\mu(\Delta m^2_{21} = 0)}{N_{\mu 0}} = -\overline{P}_{e2}c^2_{23}(c^2_{23} - \frac{1}{\bar{r}}), \quad (16)$$

where N_{e0} and $N_{\mu 0}$ are the expected number of electron and muon-like events in the absence of oscillations in the relevant energy and angular bin and $N_\mu(\Delta m^2_{21} = 0)$ is the expected number of muon-like events for $\Delta m^2_{21} = 0$. For sub-GeV events, for which which for $\Delta m^2 \ll 2E_\nu V_e$:

$$P_{e2} = \sin^2 2\theta_{12} \left(\frac{\Delta m^2_{21}}{2E_\nu V_e}\right)^2 \sin^2 \frac{V_e L}{2}. \quad (17)$$

According to Eqs. (15) and (16) the sign of the shift in the number of predicted events is opposite for electron and muon-like events and it depends on the factor $c^2_{23} - \frac{1}{\bar{r}} (\sim c^2_{23} - 0.5$ for sub-GeV events). So for θ_{23} in the first octant, $c^2_{23} > 0.5$, there is an increase (decrease) in the number of electron (muon) events as compared to the $\Delta m^2_{21} = 0$ case, while for θ_{23} in the second octant the opposite holds – just opposite to the behavior for $\theta_{13} \neq 0$. We also see that the net shift is larger for electron events than for muon events by a factor $c^2_{23}/\bar{r}$. In summary, for sub-GeV electrons, the shift in the expected number of events is proportional to the deviation of θ_{23} from maximal mixing and to $(\Delta m^2_{21})^2$, it is very weakly dependent on the zenith angle, and it decreases with the energy.

The present data may already give some hint of deviation of the 2-3 mixing from maximal. Indeed, there is some excess of the $e-$like events in the sub-GeV range. The excess increases with decrease of energy within the sample as expected from a Δm^2_{21} effect. To illustrate this I show in Fig. 3 the results of the global analysis of ATM and CHOOZ data in the framework of 3ν oscillations taking into account also the effect of Δm^2_{21} oscillations [10].

From the figure we see that, even with the present uncertainties, the ATM data has some sensitivity to Δm^2_{21} oscillation effects and that these effects break the symmetry in θ_{23} around maximal mixing. Although statistically not very significant, this preference for non-maximal 2-3 mixing is a physical effect on the present neutrino data, induced by the fact than an excess of events is observed in sub-GeV electrons but not in sub-GeV muons nor, in the same amount, in the multi-GeV electrons. As a consequence, this excess cannot be fully explained by a combination of a global rescaling and a "tilt" of the fluxes within the assumed uncertainties.

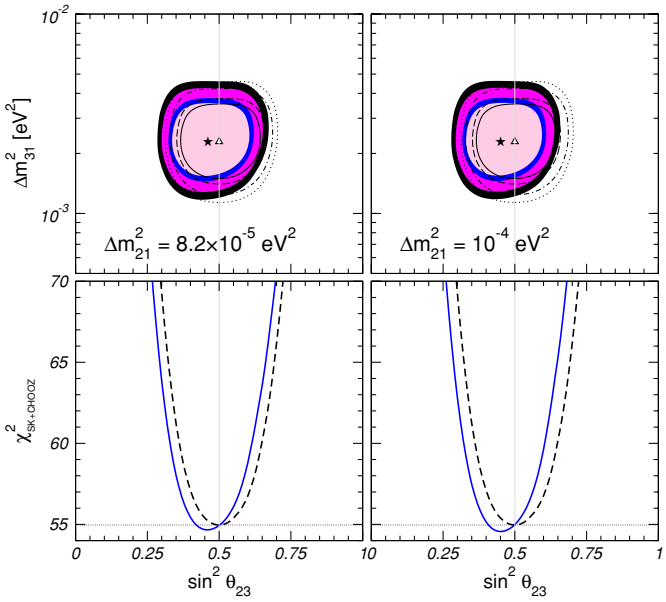

Fig 3. Effect of Δm^2_{21} oscillations on the allowed regions of the oscillation parameters Δm^2_{31} and $\sin^2\theta_{23}$ from the combined analysis of all the ATM and CHOOZ data samples. In the lower panels we show the dependence of the χ^2 function on θ_{23}, marginalized with respect to Δm^2_{31}. Hollow and dashed black lines are for $\Delta m^2_{21} = 0$. In all curves $\tan^2\theta_{12} = 0.42$

2.3. Interference of θ_{13} and Δm^2_{21} effects

Finally I would like to make some brief comment on the possible effects due to the interference between θ_{13}- and Δm^2_{21}-induced oscillations [7, 11] which could give sensitivity to the CP violating phase δ. This effect is most important for sub-GeV energies for which one can write:

$$\frac{N_e}{N_e^0} - 1 \simeq \overline{P_{e2}}\overline{r}(c_{23}^2 - \frac{1}{\overline{r}}) + 2\tilde{s}_{13}^2\overline{r}(s_{23}^2 - \frac{1}{\overline{r}}) - \overline{r}\tilde{s}_{13}\tilde{c}_{13}^2 \sin 2\theta_{23}(\cos\delta\ \overline{R_2} - \sin\delta\overline{I_2}) \quad (18)$$

where

$$P_{e2} = \sin^2 2\theta_{12,m} \sin^2\frac{\phi_m}{2} \qquad \tilde{\theta}_{13} \approx \theta_{13}\left(1 + \frac{2E_\nu V_e}{\Delta m^2_{32}}\right) \quad (19)$$

$$R_2 = -\sin 2\theta_{12,m}\cos 2\theta_{12,m}\sin^2\frac{\phi_m}{2} \qquad I_2 = -\frac{1}{2}\sin 2\theta_{12,m}\sin\phi_m$$

ϕ_m is the phase oscillation in matter and $\theta_{12,m}$ is 12 the mixing angle in matter (Eq. (13)). Fig. 4 illustrates the possible size of this effect.

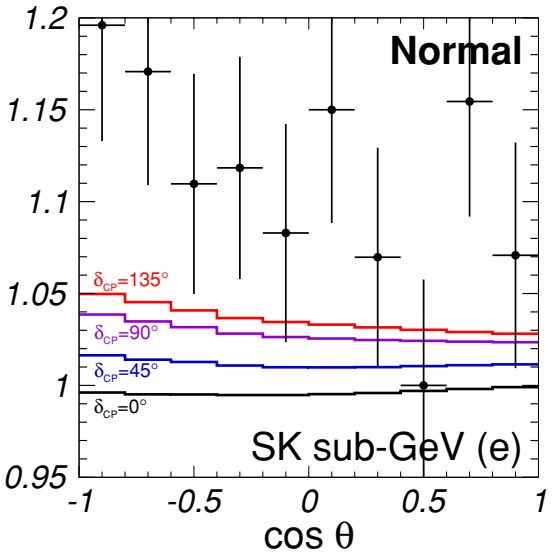

Fig 4. Sub-leading effect due to the interference of Δm^2_{21}- and θ_{13}-induced ν_e oscillations in the expected zenith angular distribution of e-like events. The curves are for CP phase given in the figure and $\sin^2\theta_{13} = 0.04$, $\sin^2\theta_{23} = 0.35$, $\tan^2\theta_{12} = 0.42$, $\Delta m^2_{21} = 1\times10^{-4}$ eV^2 and $\Delta m^2_{32} = 2.2\times10^{-3}$ eV^2.

3. Sensitivity of Future Experiments to Δm^2_{21} Oscillations

I now summarize our results of Ref. [10] on the expected sensitivity at future ATM experiments. For concreteness we assumed a SK-like detector with either 20 (SK×20) or 50 (SK×50) times the present SK-I statistics and the same systematics as SK-I, and we have used the same event samples as in SK.

First we simulate the signal according to the expectations from some specific choice of the "true" values of parameters which we denote by $\overline{\omega}$

$$\overline{\omega} \equiv (\Delta\overline{m}^2_{21},\, \Delta\overline{m}^2_{31},\, \overline{\theta}_{12},\, \overline{\theta}_{13},\, \overline{\theta}_{23})\,, \tag{20}$$

and then we construct

$$\chi^2_{\rm SK}(\Delta m^2_{21},\, \Delta m^2_{31},\, \theta_{12},\, \theta_{13},\, \theta_{23}\,|\,\overline{\omega}) \tag{21}$$

assuming 20 or 50 times the present SK statistics and three choices for the theoretical and systematic errors.

(A) same theoretical and systematic errors as in present SK;
(B) same systematic errors as in present SK, but no theoretical uncertainties;
(C) neither theoretical nor systematic uncertainties (perfect experiment).

Next, in order to study the effect that non-zero values of $\Delta\overline{m}^2_{21}$ and $\overline{\theta}_{12}$ can

produce in the determination of the ATM parameters Δm^2_{31} and θ_{23} we define

$$\chi^2_{\rm atm+reac}(\Delta m^2_{31},\, \theta_{23}\,|\,\overline{\omega}) \equiv \min_{\Delta m^2_{21},\theta_{13}} \Big[\chi^2_{\rm SK}(\Delta m^2_{21},\, \Delta m^2_{31},\, \theta_{12}=\overline{\theta}_{12},\, \theta_{13},\, \theta_{23}\,|\,\overline{\omega}) + \chi^2_{\rm chooz}(\Delta m^2_{21},\, \Delta m^2_{31},\, \theta_{12}=\overline{\theta}_{12},\, \theta_{13}\,|\,\overline{\omega}) + \left(\frac{\Delta m^2_{21}-\Delta\overline{m}^2_{21}}{\sigma_{\Delta m^2_{21}}}\right)^2\Big] \tag{22}$$

where we minimize with respect to the solar and reactor parameters Δm^2_{21} and θ_{13} and we keep only the explicit dependence on the parameters Δm^2_{31} and θ_{23}. The assumption $\theta_{12} = \overline{\theta}_{12}$ is made for purely practical reasons because a complete scan of the whole five-dimensional parameter space requires too much computer time. Note that regardless of the specific assumptions on the 'true values' $\Delta\overline{m}^2_{21}$ and $\overline{\theta}_{13}$ the parameters Δm^2_{21} and θ_{13} are allowed to vary in our fit. In the definition of $\chi^2_{\rm atm+reac}$ in Eq. (22) we have included also the CHOOZ experiment $\chi^2_{\rm chooz}$ in order to have a realistic bound on θ_{13}. Similarly, the term $[(\Delta m^2_{21} - \Delta\overline{m}^2_{21})/\sigma_{\Delta m^2_{21}})]^2$ accounts for the bound on Δm^2_{21} which is expected from KamLAND in the next few years. We have assumed that by then $\Delta\overline{m}^2_{21}$ will be known with an uncertainty of 3% at 1σ.

As an illustration of the expected sensitivity from future ATM neutrino experiments, we show in Fig. 5 the allowed regions obtained from $\chi^2_{\rm atm+reac}$ assuming 20 times the present SK statistics and the same theoretical and systematic errors as in present SK (case A). For definiteness, we choose $\overline{\theta}_{13} = 0$, $\Delta\overline{m}^2_{21} = 8.2\times10^{-5}$ eV^2 and $\tan^2\overline{\theta}_{12} = 0.42$, and we scan different values of $\Delta\overline{m}^2_{31}$ and $\overline{\theta}_{23}$. From this figure we find that:

- future ATM neutrino experiments can observe and measure deviations of θ_{23} from maximal mixing, provided that θ_{23} is not too close to 45°: $\sin^2\theta_{23} < 0.38$ or $\sin^2\theta_{23} > 0.60$; future reduction in the theoretical errors will further improve the sensitivity;
- they can discriminate between the "light-side" and "dark-side" for θ_{23}, *i.e.*, they are sensitive to the octant of θ_{23}.

In order to quantify the sensitivity of a future ATM experiment to deviation for maximal θ_{23} mixing, we have constructed the following function:

$$\Delta\chi^2_{\rm no-max}(\overline{\omega}) \equiv \min_{\Delta m^2_{31},\theta_{23}} \Big[\chi^2_{\rm atm+reac}(\Delta m^2_{31},\, \theta_{23}=45^\circ\,|\,\overline{\omega}) - \chi^2_{\rm atm+reac}(\Delta m^2_{31},\, \theta_{23}\,|\,\overline{\omega})\Big] \tag{23}$$

where $\chi^2_{\rm atm+reac}(\Delta m^2_{31},\, \theta_{23}\,|\,\overline{\omega})$ is given in Eq. (22). In Fig. 6 we plot the dependence of $\Delta\chi^2_{\rm no-max}$ on $\Delta\overline{m}^2_{31}$ and $\overline{\theta}_{23}$, for both $\Delta\overline{m}^2_{21} = 8.2\times10^{-5}$ eV^2 (colored regions) and $\Delta\overline{m}^2_{21} = 0$ (hollow regions). We take $\tan^2\overline{\theta}_{12} = 0.42$ and $\overline{\theta}_{13} = 0$. The blue, green and yellow regions correspond to $\Delta\chi^2_{\rm no-max} > 1$, 4 and 9, respectively. In other words, in Fig. 6 we display, for each value of $\Delta\overline{m}^2_{31}$, the range of

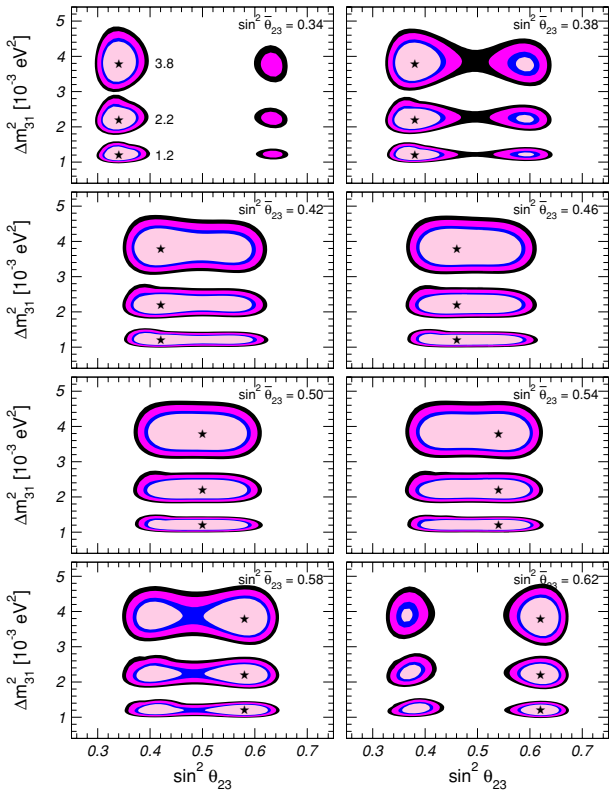

Fig 5. Allowed regions (at 90%, 95%, 99% and 3σ C.L.) of oscillation parameters Δm^2_{13} and $\sin^2\theta_{23}$ expected from an ATM neutrino experiment with 20 times the present SK statistics and the same theoretical and systematic errors as in present SK. For definiteness, we choose $\overline{\theta}_{13} = 0$, $\Delta\overline{m}^2_{21} = 8.2\times10^{-5}$ eV^2 and $\tan^2\overline{\theta}_{12} = 0.42$, and we scan different values of $\Delta\overline{m}^2_{31}$ and $\overline{\theta}_{23}$. We also include the constraints from the CHOOZ experiment, as well as the sensitivity to Δm^2_{21} expected after 3 years of KamLAND data (Eq. (22)). The undisplayed parameters Δm^2_{21} and θ_{13} are marginalized.

$\overline{\theta}_{23}$ for which the simulated signal can be reconstructed as having maximal θ_{23} at 1, 2 and 3 σ. The white region corresponds to the the range of $\overline{\theta}_{23}$ for which the simulated signal cannot be distinguished from maximal θ_{23} at 1σ.

In summary we find that the sensitivity of ATM neutrino data to deviations from maximal mixing for large values of $\Delta\overline{m}^2_{31}$ is comparable to what can be expected "after ten years" from LBL experiments according to Ref. [12], $D_{23} \leq 0.050\,(0.069)$ at 90% (3σ) CL. Furthermore, for small values of $\Delta\overline{m}^2_{31}$ the ATM neutrino studies are much more sensitive than LBL experiments, which lose sensitivity very fast when $\Delta\overline{m}^2_{31} \leq 2\times10^{-3}$ eV^2 while the bound which can be obtained from the ATM neutrino data is practically independent of the value of

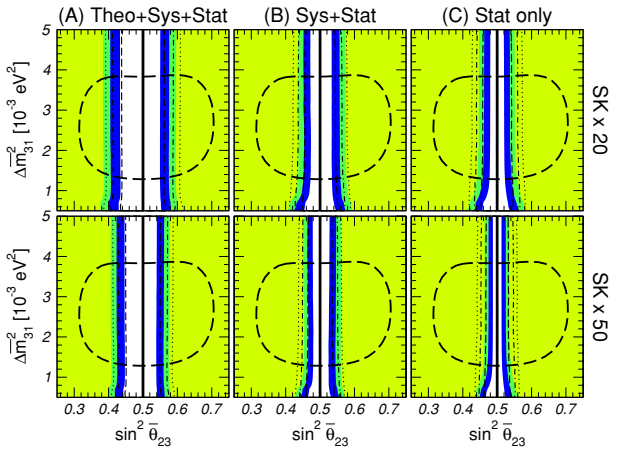

Fig 6. $(\Delta\overline{m}^2_{31}, \overline{\theta}_{23})$ regions with $\Delta\chi^2_{\rm no-max}$ smaller than 1 (white), between 1 and 4 (blue), between 4 and 9 (green), and larger than 9 (blue), respectively for $\Delta\overline{m}^2_{21} = 8.2 \times 10^{-5}$ eV^2 (the hollow regions are obtained for $\Delta\overline{m}^2_{21} = 0$). We set $\overline{\theta}_{13} = 0$ and $\tan^2\overline{\theta}_{12} = 0.42$. The dashed oval marks the 3σ region presently preferred by SK data.

$\Delta\overline{m}^2_{31}$.

The comparison among the left, central and right panels of Fig. 6 also shows that the sensitivity of ATM neutrino data to deviations from maximal mixing improves considerably if theoretical errors on the ATM fluxes and cross sections are reduced. On the contrary setting to zero the systematic uncertainties induce a smaller improvement. This implies that the obtained results hold even if the future ATM neutrino experiment is affected by somewhat larger systematics than the present SK detector has.

We also see that, as expected, when $\Delta\overline{m}^2_{21} \neq 0$ the ranges of $\overline{\theta}_{23}$ can be asymmetric. This effect is mostly seen in the first two panels (cases A and B) because larger errors allow for larger values of $\overline{D}_{23}$. We find that the overall effect of the theoretical errors is such that the fit for maximal mixing is "less-bad" if an excess of e-like sub-GeV events is observed as compared to the observation of a deficit, while for systematic uncertainties the opposite holds.

In any case, comparing the solid (obtained with $\Delta\overline{m}^2_{21} = 8.2 \times 10^{-5}$ eV^2) and the hollow (obtained with $\Delta\overline{m}^2_{21} = 0$) regions in Fig. 6 we see that the value of the solar mass splitting is not the most important effect in the discrimination from maximal mixing, and the bound comes mainly from muon data. Only when both theoretical and systematic uncertainties are neglected (case C) the bound on D_{23} becomes visibly sensitive to Δm^2_{21}. This occurs because the effect of a non-zero value of Δm^2_{21} is comparable to the small statistical error so this small

effect is relevant only when the fit is purely statistics-dominated.

In general, the sub-dominant Δm^2_{21} effect is mostly important to determine the octant of θ_{23}. For example for SK×50 the octant of θ_{23} can be determined at 90% CL if

$$\begin{array}{llll} \sin^2\theta_{23} & \leq 0.42\ [\theta_{23} \leq 40^\circ] & \text{or} \quad \sin^2\theta_{23} & \geq 0.57\ [\theta_{23} \geq 49^\circ] \qquad \text{(A)} \\ \sin^2\theta_{23} & \leq 0.48\ [\theta_{23} \leq 43^\circ] & \text{or} \quad \sin^2\theta_{23} & \geq 0.52\ [\theta_{23} \leq 46^\circ] \qquad \text{(B)} \\ \sin^2\theta_{23} & \leq 0.49\ [\theta_{23} \leq 44.4^\circ] & \text{or} \quad \sin^2\theta_{23} & \geq 0.51\ [\theta_{23} \leq 45.6^\circ] \qquad \text{(C)} \end{array}$$

These results are almost independent of the exact value of $\Delta\overline{m}^2_{31}$ within the present ATM region. From

4. New Physics Effects in Atmospheric Neutrino Oscillations

Oscillations are not the only possible mechanism for ATM $\nu_\mu \to \nu_\tau$ flavour transitions. These can also be generated by a variety of nonstandard neutrino physics characterized by the presence of an unconventional interaction (other than the neutrino mass terms) that mixes neutrino flavours. Examples include violations of the equivalence principle (VEP) [13, 14], non-standard neutrino interactions with matter [15], neutrino couplings to space-time torsion fields [16], violations of Lorentz invariance (VLI) [17, 18] and of CPT symmetry [19, 20, 21]. From the point of view of neutrino oscillation phenomenology, a critical feature of these scenarios is a departure from the $\lambda \propto E$ dependence of the conventional oscillation wavelength. Although these scenarios no longer explain the data[22, 23], a combined analysis of the ATM neutrino and K2K data can be performed to obtain the best constraints to-date on the size of sub-dominant oscillation effects [22, 1].

We concentrate on new physics (NP) effects affecting ν_μ–ν_τ flavour mixing with a strength which is constant along the neutrino trajectory. In this case the oscillation probabilities of neutrinos (+) and antineutrinos (−) take the form [20]:

$$P_{\nu_\mu\to\nu_\mu} = 1 - P_{\nu_\mu\to\nu_\tau} = 1 - \sin^2 2\Theta\, \sin^2\left(\frac{\Delta m^2 L}{4E}\,\mathcal{R}\right), \tag{24}$$

with

$$\begin{array}{ll} \sin^2 2\Theta & = \frac{1}{\mathcal{R}^2}\left(\sin^2 2\theta + R_n^2 \sin^2 2\xi_n + 2R_n \sin 2\theta \sin 2\xi_n \cos\eta_n\right), \\ \mathcal{R} & = \sqrt{1 + R_n^2 + 2R_n\left(\cos 2\theta \cos 2\xi_n + \sin 2\theta \sin 2\xi_n \cos\eta_n\right)}, \\ R_n & = \sigma_n^+ \frac{\Delta\delta_n E^n}{2}\,\frac{4E}{\Delta m^2}. \end{array} \tag{25}$$

Δm^2 is the mass-squared difference between the two neutrino mass eigenstates, $\sigma_n^\pm$ accounts for a possible relative sign of the NP effects between neutrinos and

antineutrinos, and $\Delta\delta_n$ parametrizes the size of the NP terms. θ is the mass-flavour mixing angle and ξ_n is the NP-flavour mixing angle and η_n is the possible non-vanishing relative phase. We have assumed scenarios with one NP source characterized by a unique $\Delta\delta_n$.

Eq. (24) describes, for example, flavour oscillations due to new tensor-like interactions for which $n = 1$, leading to a contribution to the oscillation wavelength inversely proportional to the neutrino energy. This is the case for ν_μ and ν_τ's of different masses in the presence of violation of the equivalence principle (VEP) due to non- universal coupling of the neutrinos, $\gamma_1 \neq \gamma_2$ (ν_1 and ν_2 being related to ν_μ and ν_τ by a rotation ξ_{vep}), to the local gravitational potential ϕ [13, 14].

For constant potential ϕ, this mechanism is phenomenologically equivalent to the breakdown of Lorentz invariance resulting from different asymptotic values of the velocity of the neutrinos, $c_1 \neq c_2$, with ν_1 and ν_2 being related to ν_μ and ν_τ by a rotation ξ_{vli} [17, 18].

For vector-like interactions, $n = 0$, the oscillation wavelength is energy-independent. This may arise, for instance, from a non-universal coupling of the neutrinos, $k_1 \neq k_2$ (ν_1 and ν_2 is related to the ν_μ and ν_τ by a rotation ξ_Q), to a space-time torsion field Q [16]. Violation of CPT resulting from Lorentz-violating effects such as the operator, $\bar{\nu}_L^\alpha b_\mu^{\alpha\beta}\gamma_\mu\nu_L^\beta$, also lead to an energy independent contribution to the oscillation wavelength [19, 20, 21] which is a function of the eigenvalues of the Lorentz violating CPT-odd operator, b_i, and the rotation angle, $\xi_{\not{C}\mathrm{PT}}$, between the corresponding neutrino eigenstates ν_i and the flavour eigenstates ν_α.

The flavour oscillations of ATM ν_μ' s in these scenarios is described by Eq. (24) with the identification:

$$\begin{array}{lll}
\xi_1 = \xi_{vep} & \Delta\delta_1 = 2|\phi|(\gamma_1 - \gamma_2) \leq 1.6 \times 10^{-24}\,, & \text{for VEP} \\
\xi_1 = \xi_{vli}\,, & \Delta\delta_1 = (c_1 - c_2) \equiv\leq 1.6 \times 10^{-24}\,, & \text{for VLI} \\
\xi_0 = \xi_Q\,, & \Delta\delta_0 = Q(k_1 - k_2) \leq 6.3 \times 10^{-23}\ \mathrm{GeV}\,, & \text{for coupling to torsion} \\
\xi_0 = \xi_{\not{C}\mathrm{PT}}\,, & \Delta\delta_0 = b_1 - b_2 \leq 5.0 \times 10^{-23}\ \mathrm{GeV}\ , & \text{for } \not{C}\text{PT}\,,\ \text{VLI}
\end{array} \tag{26}$$

where for the first three scenarios $\sigma^+ = \sigma^-$ while for the CPT violating case $\sigma^+ = -\sigma^-$.

In the left panels of Fig. 7 we illustrate the effect of the presence of the NP in the ATM neutrino events distributions for Δm^2 oscillations (Δm^2-OSC) plus sub-dominant NP effects, for some characteristic values of the NP-parameters. In all cases R_n is a growing function of E and the NP effects become relevant in the higher energy samples, in particular for upward going muons.

At present the strongest limits on NP neutrino oscillations arise from the non-observation of departure from the Δm^2_{23} oscillation behaviour in ATM neu-

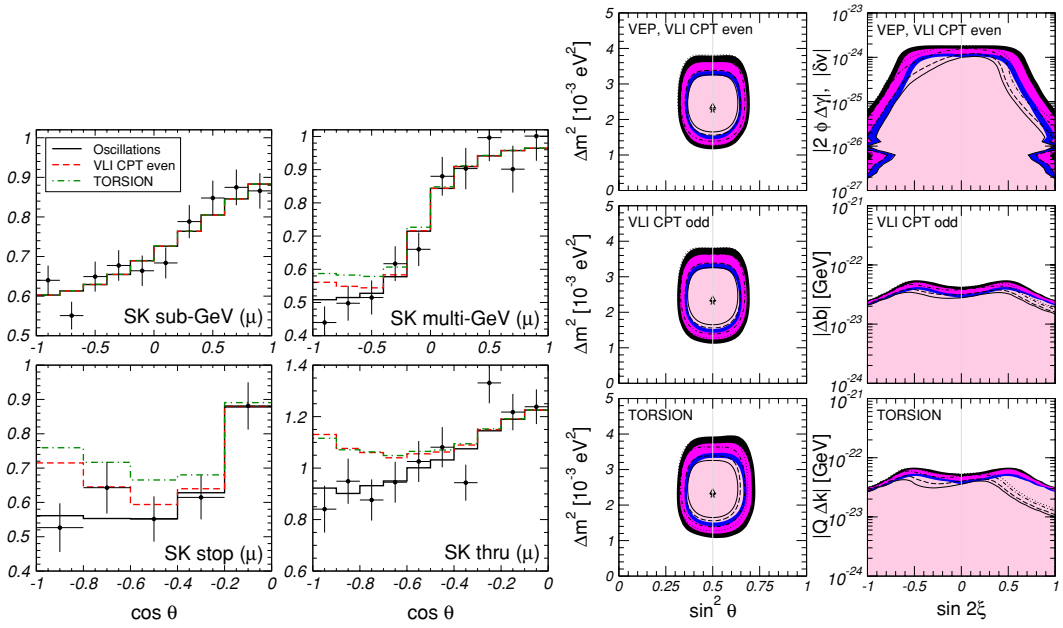

Fig 7. **Left** Zenith-angle distributions (normalized to the no-oscillation prediction) for the SK μ-like events. The full line gives the distribution for the best fit of Δm^2-OSC, $\Delta m^2 = 2.2 \times 10^{-3}$ eV^2 and $\sin^2\theta = 0.5$. The dashed and dotted lines give the distributions for Δm^2-OSC+NP scenarios for $n = 1$ and $n = 0$ with $\Delta\delta_1 = 2.0 \times 10^{-24}$ and $\Delta\delta_0 = 4.2 \times 10^{-23}$ GeV respectively. In both cases $\eta = \xi = 0$ and the oscillation parameters have been set to their best fit values. **Right** Allowed parameter regions for the analysis of ATM and K2K data in presence of $\nu_\mu \to \nu_\tau$ oscillations and different NP effects as labeled in the figure. Each panel shows a two-dimensional projection of the allowed five-dimensional region after marginalization with respect to the three undisplayed parameters. The different contours correspond to the two-dimensional allowed regions at 90%, 95%, 99% and 3σ CL.

trinos and SK and the confirmation from K2K.

In the right panels of Fig. 7 we plot two-dimensional projections of the allowed parameter region for the analysis of ATM and K2K data in presence of $\nu_\mu \to \nu_\tau$ oscillations and different NP effects.

Several comments are in order. First, from the figures we see that the best fit point for the global Δm^2-OSC+NP scenarios is always very near the best fit point of pure Δm^2-OSC. In other words, the data does not show any evidence of presence of NP even as a sub-dominant effect. Second, the figures illustrate the robustness of the allowed ranges of mass and mixing derived from the analysis of ATM and K2K data under the presence of these generic NP effects. Third the analysis allow us to derive well-defined upper bounds on the NP strength. In Eqs.(26) we quote the 3σ bounds from this up-to-date combined analysis of SK and K2K data performed in Ref.[1].

5. Some Final Remarks

In this talk I have presented the basic features of sub-leading effects in ATM neutrino oscillations due to three-neutrino oscillation effects as well as to more exotic forms of new physics. We have seen that a high statistics ATM neutrino experiment can give important information on:

(a) the possible deviation of θ_{23} from maximal mixing from leading Δm^2_{23}- and sub-dominant Δm^2_{21}- and θ_{13}-induced effects;
(b) the octant of θ_{23} from sub-dominant Δm^2_{21} effects;
(c) the mass ordering from sub-dominant θ_{13} effects if large;
(d) CP violation from interference of sub-dominant Δm^2_{21} and θ_{13} effects;
(e) new physics effects in neutrino propagation.

I will end this talk with Fig. 8 where I show the results of the ATM neutrino analysis in terms of leading $\nu_\mu \to \nu_\tau$ oscillations when some of the errors discussed in the introduction are removed.

Obviously, removing some sources of errors as shown in Fig. 8 is not realistic. The aim of this figure is to illustrate that, even what we know about the ATM leading neutrino oscillations, relies on the assumed theoretical and experimental systematic uncertainties. All the sub-leading effects discussed here modify the leading oscillation results at most at the few percent level. Therefore their observability depends even more strongly on the precision attainable for the theoretical and systematic uncertainties which is the subject of most of the talks and discussions in this workshop.

I want to thank my collaborators on the subject M. Maltoni and A.Y. Smirnov. I am particularly indebted to M. Maltoni for his help in preparing the

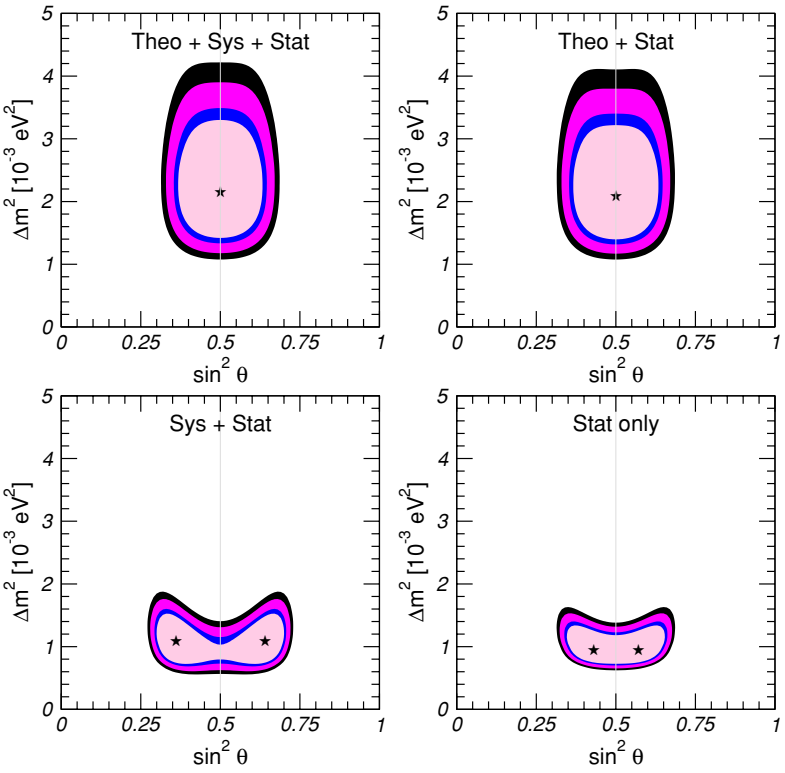

Fig 8. Allowed regions for the ATM neutrino analysis in terms of leading $\nu_\mu \rightarrow \nu_t au$ oscillations for several combinations of the theoretical and experimental systematic errors.

talk and his careful reading of the manuscript. This work was supported by the NSF grant PHY0098527 and by Spanish Grant No FPA-2004-00996.

References

[1] M. C. Gonzalez-Garcia and M. Maltoni, Phys. Rev. D **70**, 033010 (2004).
[2] M. Honda, T. Kajita, K. Kasahara and S. Midorikawa, Phys. Rev. D **70**, 043008 (2004).
[3] See talk by E. Lisi in these proceedings and references therein.
[4] J. T. Pantaleone, Phys. Rev. D **49**, 2152 (1994)
[5] E. Kh. Akhmedov, A. Dighe, P. Lipari, A. Yu. Smirnov, Nucl. Phys. **B542**, 3 (1999).
[6] M. Chizhov, M. Maris and S. T. Petcov, hep-ph/9810501.
[7] M. C. Gonzalez-Garcia and M. Maltoni, Eur. Phys. J. C **26**, 417 (2003).
[8] J. Bernabeu, S. Palomares Ruiz and S. T. Petcov, Nucl. Phys. B **669**, 255 (2003); S. Palomares-Ruiz and S. T. Petcov, Nucl. Phys. B **712**, 392 (2005).
[9] O.L.G. Peres and A.Yu. Smirnov, Phys. Lett. **B456**, 204 (1999).
[10] M. C. Gonzalez-Garcia, M. Maltoni and A. Y. Smirnov, Phys. Rev. D **70**, 093005 (2004)
[11] O.L.G. Peres, A.Yu. Smirnov, Nucl. Phys. **B680** 479, (2004).
[12] S. Antusch, P. Huber, J. Kersten, T. Schwetz and W. Winter, hep-ph/0404268.
[13] M. Gasperini, Phys. Rev. D **38** (1988) 2635; Phys. Rev. D **39**, 3606 (1989);
[14] A. Halprin and C.N. Leung, Phys. Rev. Lett. **67**, 1833 (1991).
[15] L. Wolfenstein, Phys. Rev. **D17**, 236 (1978)
[16] V. De Sabbata and M. Gasperini, Nuovo Cimento A **65**, 479 (1981).
[17] S. Coleman and S.L. Glashow, Phys. Lett. B **405**, 249 (1997).
[18] S.L. Glashow, A. Halprin, P.I. Krastev, C.N. Leung, and J. Pantaleone, Phys. Rev. D **56**, 2433 (1997).
[19] D. Colladay and V.A. Kostelecky, *Phys. Rev.* **D55**, 6760 (1997).
[20] S. Coleman and S.L. Glashow, Phys. Rev. D **59**, 116008 (1999).
[21] V. D. Barger, S. Pakvasa, T. J. Weiler and K. Whisnant, Phys. Rev. Lett. **85**, 5055 (2000)
[22] G. L. Fogli, E. Lisi, A. Marrone and G. Scioscia, Phys. Rev. D **60**, 053006 (1999)
[23] N. Fornengo, M. C. Gonzalez-Garcia and J. W. F. Valle, JHEP **0007** (2000) 006.